

Observational constraints on Chaplygin cosmology in a braneworld scenario with induced gravity and curvature effect

Kourosh Nozari^{a,b,1}, T. Azizi^{a,2} and N. Alipour^{a,3}

^a*Department of Physics, Faculty of Basic Sciences, University of Mazandaran,
P. O. Box 47416-95447, Babolsar, IRAN*

^b*Research Institute for Astronomy and Astrophysics of Maragha,
P. O. Box 55134-441, Maragha, IRAN*

Abstract

We study cosmological dynamics and late-time evolution of an extended induced gravity braneworld scenario. In this scenario, curvature effects are taken into account via the Gauss-Bonnet term in the bulk action and there is also a Chaplygin gas component on the brane. We show that this model mimics an effective phantom behavior in a relatively wider range of redshifts than previously formulated models. It also provides a natural framework for smooth crossing of the phantom-divide line due to presence of the Chaplygin gas component on the brane. We confront the model with observational data from type Ia Supernovae, Cosmic Microwave Background and Baryon Acoustic Oscillations to constraint the model parameters space.

PACS: 98.80.-k, 95.36.+x, 98.80.Cq

Key Words: Cosmology: Dark energy -Cosmology: theory- Cosmology: Observations

¹knozari@umz.ac.ir

²t.azizi@umz.ac.ir

³n.alipour@umz.ac.ir

1 Introduction

The outcome of supernovae redshift-luminosity distance and also other observational probes, that the universe is undergoing an accelerated phase of expansion, has stimulated a lot of attempt to explain this unexpected feature. Since dynamics of the universe is described by the Friedmann equation which follows from the Einstein field equations in four dimensions, all modifications of the Friedmann equation ultimately affect the Einstein field equations too. In this respect, modifications to geometric part of the field equations imply some sort of alternative geometries, while modifications to matter sector of the theory involve new forms of energy densities that have not been observed yet. In fact, the geometric part of the Einstein's field equations can be modified to incorporate *dark geometry* as $G_{\mu\nu} + G_{\mu\nu}^{(Dark)} = 8\pi G T_{\mu\nu}^{(M)}$. In the same way and within the second viewpoint, Einstein's field equations can be written as $G_{\mu\nu} = 8\pi G (T_{\mu\nu}^{(M)} + T_{\mu\nu}^{(Dark)})$ where $T_{\mu\nu}^{(M)}$ and $T_{\mu\nu}^{(Dark)}$ are energy-momentum tensor of ordinary matter and dark energy respectively.

Within the first viewpoint, a well-studied model of modified gravity is the Dvali- Gabadadze-Porrati (DGP) braneworld scenario (G. Dvali, G. Gabadadze & M. Porrati 2000; G. Dvali et al. 2000; A. Lue 2006), in which our four-dimensional world is a FRW 3-brane embedded in a five-dimensional Minkowski bulk. The model is characterized by a cross-over length scale r_c such that gravity is a four-dimensional theory at scales $r \ll r_c$ where matter behaves as pressureless dust. In the self-accelerating DGP branch gravity leaks out into the bulk at scales $r \gg r_c$ and the cosmology approaches the behavior of a cosmological constant (C. Deffayet 2001; C. Deffayet, G. Dvali & G. Gabadadze 2002). In the self-decelerating, normal DGP branch, gravity leaks in from the bulk at scales $r \gg r_c$, leading to a cosmology which is in contrast to the observed late-time acceleration.

Cosmological dynamics in a braneworld setup that treats Gauss-Bonnet curvature effect and the DGP induced gravity in a unified manner, has been studied recently (G. Kofinas, R. Maartens & E. Papantonopoulos 2003; R. A. Brown et al. 2005; R. -G. Cai, H. -S. Zhang & A. Wang 2005; R. A. Brown 2007; H. Maeda, V. Sahni & Y. Shtanov 2007; J. -H. He, B. Wang & E. Papantonopoulos 2007; K. Nozari & B. Fazlpour 2008; K. Nozari & N. Rashidi 2009). This model which is called GBIG-gravity, is a generalized braneworld scenario that contains both UV (ultra-violet) and IR (infra-red) limits in a unified manner: It contains stringy effect via the Gauss-Bonnet (GB) term in the bulk action as the UV sector of the theory and Induced Gravity (IG) effect which becomes important in the IR limit. The cosmological dynamics and possible realization of the phantom-like behavior in this setup are studied recently (M. Bouhmadi-Lopez & P. V. Moniz (2008, 2009); K. Nozari and N. Rashidi 2009; K. Nozari, T. Azizi & M. R. Setare 2009; K. Nozari & N. Aliopur 2009).

Within the second viewpoint and focusing on the matter sector of the Einstein field equations, a well-studied model introduces into $T_{\mu\nu}$ a dark energy component called the Chaplygin gas (A. Dev, J. S. Alcaniz & D. Jain 2003; L. Amendola et al. 2003; O. Bertolami et al. 2004; M. Biesiada, W. Godlowski & M. Szydlowski 2005; X. Zhang, F. Wu & J. Zhang 2006; H. Zhang & Z. -H. Zhu 2006; Heydari-Fard & H. R. Sepangi 2008; H. Zhang, Z. -H. Zhu & L. Yang 2009; M. H. Mohseni Sadjadi 2009). This model is similar to the DGP model in the sense that it is also characterized by a cross-over length scale below which the gas behaves as pressureless dust, and above which it approaches the behavior of a cosmological constant. This length scale is expected to be of the same order of magnitude as the r_c scale of the DGP model (M. Roos 2007). Accelerating Chaplygin gas combined with the decelerating braneworld DGP model can produce an overall accelerated expansion of the order of magnitude seen (M. Roos (2007, 2008a,b); M. Bouhmadi-Lopez & R. Lazkoz 2007). However, both the self-accelerating

DGP model in flat space and the standard Chaplygin gas model have problems in fitting with present supernovae data (T. M. Davis 2007).

Recently, astronomical observations with WMAP7 have indicated that the equation of state parameter of dark energy can be less than -1 and even can display a transient behavior (E. Komatsu et al. 2010). A simple way to explain this phenomenon is to consider a non-canonical phantom dark energy (R. R. Caldwell 2002), that introduces new theoretical facilities and challenges in this field. Phantom fields are a sort of scalar fields with negative sign for the kinetic energy term. Indeed, phantom fields suffer from instabilities due to violation of the null energy condition, and a phantom universe eventually ends up with a Big Rip singularity (R. R. Caldwell, M. Kamionkowski & N. N. Weinberg). Thus it follows immediately that there must be some alternative approaches to realize a phantom-like behavior without introducing any phantom field in the model. With phantom-like behavior, we mean the growth of the effective dark energy density with cosmic time and in the same time, the effective equation of state parameter should stay always less than -1 . In this regard, it has been shown that the normal, non-self-accelerating branch of the DGP scenario has the potential to explain the phantom-like behavior without introducing any phantom fields on the brane (V. Sahni & Y. Shtanov 2003; A. Lue & G. D. Starkman 2004; R. Maartens & E. Majerotto 2006). The main problem associated to this model and its extended versions (L. P. Chimento, R. Lazkoz, R. Maartens 2006; M. Bouhmadi-Lopez & P. V. Moniz 2008) is that the effective phantom picture always breaks down at some point as the effective dark energy density will cease to be positive at a redshift in the past.

With these preliminaries, in this paper we study cosmological dynamics and late-time evolution of an extended induced gravity braneworld scenario. In this scenario, curvature effects are taken into account via the Gauss-Bonnet term in the bulk action and there is also a Chaplygin gas component on the brane. Our motivation for incorporation of the GB correction in the DGP setup is that the DGP model gives just the infra-red modification of the general relativity. It would be expected that a consistent DGP braneworld model would have also ultraviolet modifications as well, associated to high-energy stringy effects at earlier times. This expectation can be fulfilled via incorporation of the GB term in the bulk action. By including a Chaplygin gas fluid on the brane, there will be no breakdown of the phantom-like prescription in this model. The presence of the Chaplygin gas component also provides a smooth crossing of the cosmological constant line in this scenario.

The paper is organized as follows: In section 2 we start from the action of the scenario and derive the corresponding Friedmann equation. Then, we study cosmological dynamics of this generalized braneworld setup and investigate possible realization of the phantom mimicry without introducing a phantom field. In section 3, we investigate possible crossing of the phantom divide line by the effective equation of state parameter and also we study dynamical screening of the brane cosmological constant. We constraint the model parameter space by using the observational data from type Ia Supernovae, Cosmic Microwave Background and Baryon Acoustic Oscillations data in section 4. Finally, our summery and conclusions are presented in section 5.

2 The setup

We start with the following action

$$S = \frac{1}{2\kappa_5^2} \int d^5x \sqrt{-g^{(5)}} \left\{ R^{(5)} - 2\Lambda_5 + \beta \left[(R^{(5)})^2 - 4R_{ab}^{(5)} R^{(5)ab} + R_{abcd}^{(5)} R^{(5)abcd} \right] \right\} \\ + \frac{r_c}{2\kappa_5^2} \int_{y=0} d^4x \sqrt{-g} \left(R - \frac{\kappa_5^2}{r_c} \lambda \right) + \mathcal{L}_m, \quad (1)$$

where the first term shows the usual Einstein-Hilbert action in 5D bulk with the Gauss-Bonnet term and β is the Gauss-Bonnet coupling constant. The assumption that β is non-negative is motivated by string theory, where typically $\beta \propto \ell_{string}^2$ (G. Kofinas, R. Maartens & E. Papantonopoulos 2003; R. A. Brown 2007). r_c is the DGP crossover scale, λ is tension of the brane, and \mathcal{L}_m is the matter field Lagrangian on the brane. In our case, \mathcal{L}_m contains ordinary matter (CDM) and a generalized Chaplygin gas component with equation of state of the form $p_{ch} = -\frac{A}{\rho_{ch}^\alpha}$. The cosmological dynamics on the brane obeys the following generalized Friedmann equation (M. Bouhmadi-Lopez & P. V. Moniz 2008, 2009; K. Nozari and N. Rashidi 2009)

$$\left[1 + \frac{8}{3}\beta \left(H^2 + \frac{\Phi}{2} + \frac{K}{a^2} \right) \right]^2 \left(H^2 - \Phi + \frac{K}{a^2} \right) = \left[r_c \left(H^2 + \frac{K}{a^2} \right) - \frac{\kappa_5^2}{6} (\rho + \rho_{ch} + \lambda) \right]^2. \quad (2)$$

The bulk contains a black hole mass and a cosmological constant, so that Φ is defined as $\Phi + 2\beta\Phi^2 = \frac{\Lambda_5}{6} + \frac{\Upsilon}{a^4}$. The bulk black hole mass originates on the bulk Weyl tensor so that the bulk reduces to Schwarzschild-AdS₅ if $\beta = 0$ and to AdS₅ if $\beta = 0 = \Upsilon$. In which follows, we restrict ourselves to the case that the bulk black hole mass vanishes, $\Upsilon = 0$, and therefore $\Phi + 2\beta\Phi^2 = \frac{\Lambda_5}{6}$. In this case the bulk cosmological constant is given by $\Lambda_5 = \frac{-6}{l^2} + \frac{12\beta}{l^4}$, where l is the bulk curvature. Assuming $\Lambda_5 = 0$ corresponding to a Minkowski bulk, for a spatially flat FRW brane ($K = 0$), the Friedmann equation would be as follows

$$\left[1 + \frac{8}{3}\beta \left(H^2 + \frac{\Phi}{2} \right) \right]^2 (H^2 - \Phi) = \left[r_c H^2 - \frac{\kappa_5^2}{6} (\rho + \rho_{ch} + \lambda) \right]^2. \quad (3)$$

With $\Lambda_5 = 0$, we find $\Phi = 0$ or $\Phi = -\frac{1}{2\beta}$. Our forthcoming arguments will be based on the choice $\Phi = 0$. Now we look at the conservation equation. In our setup, there is no energy exchange between bulk and brane. Therefore, total matter/energy budget on the brane is conserved by virtue of the Bianchi's identity so that $\dot{\rho}_{tot} + 3H(\rho_{tot} + p_{tot}) = 0$, where p_{tot} and ρ_{tot} are total pressure and energy density on the brane respectively. Restricting further so that conservation holds for two matter components separately, we have for the CDM component

$$\dot{\rho}_m + 3H\rho_m = 0 \quad (4)$$

which integrates to the usual $\rho_m = \rho_{m0}(1+z)^3$, whereas for the Chaplygin gas component, the continuity equation can be written as

$$\dot{\rho}_{ch} + 3H(\rho_{ch} + p_{ch}) = 0. \quad (5)$$

Since $p_{ch} = -\frac{A}{\rho_{ch}^\alpha}$ (M. Roos 2007; M. Bouhmadi-Lopez & R. Lazkoz 2007), we find

$$\rho_{ch} = (\rho_{ch})_0 \left[A_s + \frac{1 - A_s}{a^{3(1+\alpha)}} \right]^{\frac{1}{1+\alpha}}, \quad (6)$$

where $A_s = \frac{A}{(\rho_{ch})_0^{1+\alpha}}$. Using the definition of the redshift parameter z as $\frac{a}{a_0} = \frac{1}{1+z}$, and setting $a_0 = 1$ for convenience, we find

$$\rho_{ch} = (\rho_{ch})_0 \left[A_s + (1 - A_s)(1+z)^{3(\alpha+1)} \right]^{\frac{1}{1+\alpha}}. \quad (7)$$

This expression supports the interest on Chaplygin cosmologies since it reflects the fact that the energy density of such fluids interpolates between dust and a cosmological constant (A. Y. Kamenshchik, U. Moschella & V. Pasquier 2001; N. Bilic, G. B. Tupper & R. D. Viollier 2002; M. C. Bento, O. Bertolami & A. A. Sen 2002). After these preliminaries, we are looking for the late-time behavior of the normal branch of this chaplygin GBIG scenario. Defining the cosmological parameters as $\Omega_m = \frac{\kappa_4^2 \rho_{m0}}{3H_0^2}$, $\Omega_\Lambda = \frac{\kappa_4^2 \Lambda}{3H_0^2}$, $\Omega_{r_c} = \frac{1}{4r_c^2 H_0^2}$, $\Omega_\beta = \frac{8}{3} \beta H_0^2$ and $\Omega_{ch} = \frac{(\rho_{ch})_0 \kappa_4^2}{3H_0^2}$, the Friedmann equation on the brane, equation (3), can be expressed in a dimensionless form as follows

$$E^2(z) = -2\sqrt{\Omega_{r_c}} E(z) [1 + \Omega_\beta E^2(z)] + \Omega_m (1+z)^3 + \Omega_{ch} [A_s + (1 - A_s)(1+z)^{3(\alpha+1)}]^{\frac{1}{1+\alpha}} + \Omega_\Lambda, \quad (8)$$

where $E(z) = \frac{H}{H_0}$. We assume $0 < A_s < 1$ and $1 + \alpha > 0$. With these conditions, it is possible to realize a de Sitter phase at late time (M. Bouhmadi-Lopez & R. Lazkoz 2007). As an important ingredient of the model, the following constraint equation can be obtained from (8) by setting $z = 0$

$$1 + 2\sqrt{\Omega_{r_c}}(1 + \Omega_\beta) = \Omega_m + \Omega_{ch} + \Omega_\Lambda. \quad (9)$$

Note that based on this relation, the region $\Omega_m + \Omega_{ch} + \Omega_\Lambda < 1$ in the model parameters space is physically unacceptable. Taking the time derivative of equation (9), and using the continuity equation for matter on the brane, the Hubble rate can be deduced as follows

$$\frac{\dot{H}}{H_0^2} = -\frac{3}{2} \frac{[E(z)(1+z)^3] \left[\Omega_m + \frac{3(1-A_s)\Omega_{ch}(1+z)^{3\alpha}}{[A_s+(1-A_s)(1+z)^{3\alpha}]^{\frac{\alpha}{\alpha+1}}} \right]}{E(z) + \sqrt{\Omega_{r_c}}[1 + \Omega_\beta E^2(z)] + 2\sqrt{\Omega_{r_c}}\Omega_\beta E^2(z)}. \quad (10)$$

With the previous constraints on A_s , and assuming that $\beta \geq 0$ (motivated by string theory as $\beta \propto \ell_{string}^2$), it is obvious that this relation always has a negative value in the whole physically admissible parameters space. This feature is plotted in fig 1⁴. Since $\dot{H} < 0$, the Hubble parameter decreases as the brane expands, consequently there is no super-acceleration in this braneworld universe. Therefore, the brane does not hit a big rip singularity as its fate. Note also that \dot{H} vanishes when $z \rightarrow -1$, while H is positive at this limit. This is a reflection of late-time de Sitter character of the model. It has been shown that it is possible to have *Big Freeze* singularity in FRW universe filled with a generalized Chaplygin gas (A. V. Yurov et al. 2008; M.

⁴The numerical values of cosmological parameters used to plot figures of this paper are taken from Table 2.

Bouhmadi-Lopez, P. F. Gonzalez-Diaz & P. Martin-Moruno 2008; M. Bouhmadi-Lopez et al. (2009,2010)). So, essentially appearance of this type of singularity in our framework is probable too. Nevertheless, existence of induced gravity on the brane and the Gauss-Bonnet term in the bulk action may help to overcome this difficulty. This issue needs further investigations and we are going to study its separately. The deceleration parameter, q depends on \dot{H} through the

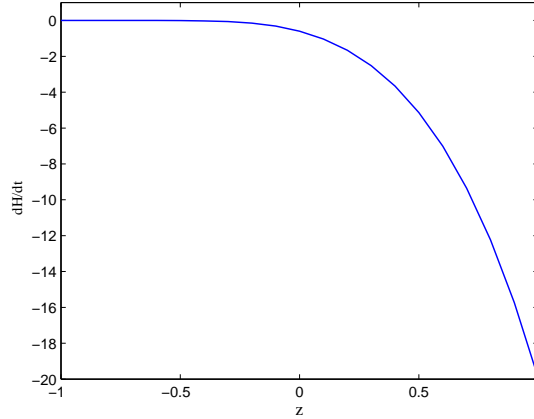


Figure 1: Variation of $\frac{\dot{H}}{H^2}$ with redshift. The parameter values to plot this figure are taken from Table 2.

relation $q = -[\frac{\dot{H}}{H^2} + 1]$, which can be expressed in the following form

$$q = -\left(1 - \frac{3}{2} \frac{\left[\frac{(1+z)^3}{E(z)}\right] \left(\Omega_m + \frac{3(1-A_s)\Omega_{cb}(1+z)^{3\alpha}}{[A_s+(1-A_s)(1+z)^{3\alpha}]^{\frac{\alpha}{\alpha+1}}}\right)}{[E(z) + \sqrt{\Omega_{rc}}(1 + \Omega_\beta E^2(z)) + 2\sqrt{\Omega_{rc}}\Omega_\beta E^2(z)]}\right). \quad (11)$$

In figure 2, the dimensionless deceleration parameter q is plotted versus the redshift for a fixed set of the parameters as are presented in table 2. In this model, the universe enters the accelerating phase at $z \approx 0.13$.

3 Crossing the phantom divide

In this section, we show that a phantom-like behavior can be realized on the brane, in a relatively wider range of redshifts than previously formulated models (see for instance R. Maartens & E. Majerotto 2006; L. P. Chimento, R. Lazkoz, R. Maartens 2006; M. Bouhmadi-Lopez & P. V. Moniz 2008). This phantom-like behavior occurs without including any phantom matter. The phantom-like prescription is based on the definition of an effective energy density which is corresponding to a balance between the cosmological constant and geometrical effects encoded in the Hubble rate evolution (V. Sahni & Y. Shtanov 2003; A. Lue & G. D. Starkman 2004; V. Sahni 2005). This behavior is based on the definition of an effective energy density ρ_{eff} , which increases with cosmic time and an effective equation of state parameter always less than -1 . More precisely, the effective description is inspired in writing down the modified Friedmann

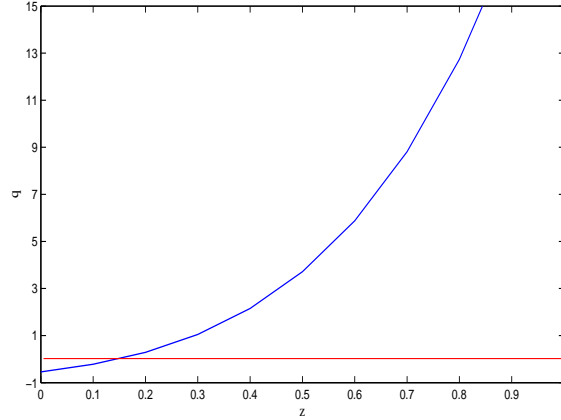


Figure 2: Variation of q versus the redshift. Parameters values are taken from Table 2.

equation of the brane as the usual 4D Friedmann equation (A. Lue & G. D. Starkman 2004; M. Bouhmadi-Lopez & P. V. Moniz 2008), so that

$$H^2 = \frac{\kappa_4^2}{3}(\rho_m + \rho_{eff}). \quad (12)$$

Using equations (8) and (12), we find

$$\rho_{eff} = \frac{3H_0^2}{\kappa_4^2} \left[-2\sqrt{\Omega_{rc}}E(z)[1 + \Omega_\beta E^2(z)] + \Omega_{ch}[A_s + (1 - A_s)(1 + z)^{3(\alpha+1)}]^{\frac{1}{1+\alpha}} + \Omega_\Lambda \right] \quad (13)$$

By definition, phantom-like prescription breaks down if $\rho_{eff} \leq 0$. Figure 3 shows variation of $\rho_{eff}^{(DE)}$ versus α and redshift in this model. The phantom-like behavior can be realized for all values of α that $1 + \alpha > 0$. Figure 4 shows variation of $\rho_{eff}^{(DE)}$ versus A_s and redshift in this model. The phantom-like behavior can be realized if $0 < A_s < 1$. Based on this analysis, ρ_{eff} is always positive and grows by cosmic expansion, and this is a typical phantom-like behavior. Note that in the absence of the Chaplygin gas component on the brane, the effective phantom picture breaks down at a redshift in the past where the effective dark energy density becomes negative. The effect of the Chaplygin component as a new ingredient added to the GBIG braneworld scenario, is that the effective phantom-like picture has no break down in this case. The main point here is the fact that it is possible essentially to save phantom-like prescription for a wide range of redshifts in this case. Now, the effective equation of state parameter ω_{eff} , can be defined using the conservation equation of the effective energy density on the brane

$$\dot{\rho}_{eff} + 3H(1 + \omega_{eff})\rho_{eff} = 0. \quad (14)$$

A straightforward calculation shows (M. Roos 2007; M. Bouhmadi-Lopez & R. Lazkoz 2007)

$$\dot{\rho}_{ch} = -\frac{9HH_0^2\Omega_{ch}(1 - A_s)(1 + z)^{3(1+\alpha)}}{[A_s + (1 - A_s)(1 + z)^{3(1+\alpha)}]^{\frac{\alpha}{\alpha+1}}}. \quad (15)$$

Then the effective energy density evolves as follows

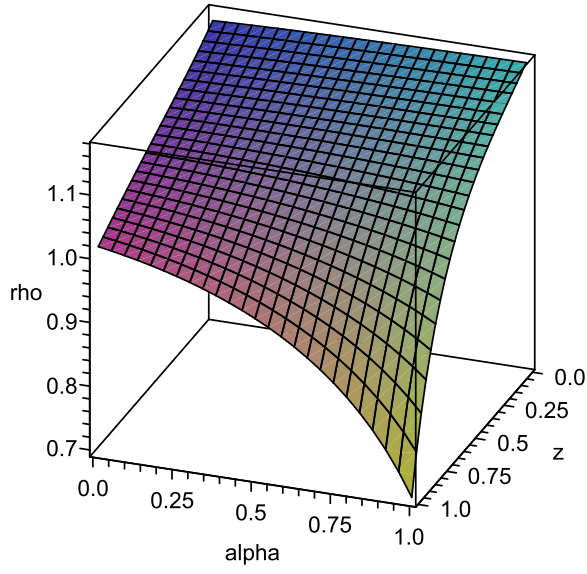


Figure 3: Variation of the effective dark energy versus α and redshift. Parameters values are taken from Table 2.

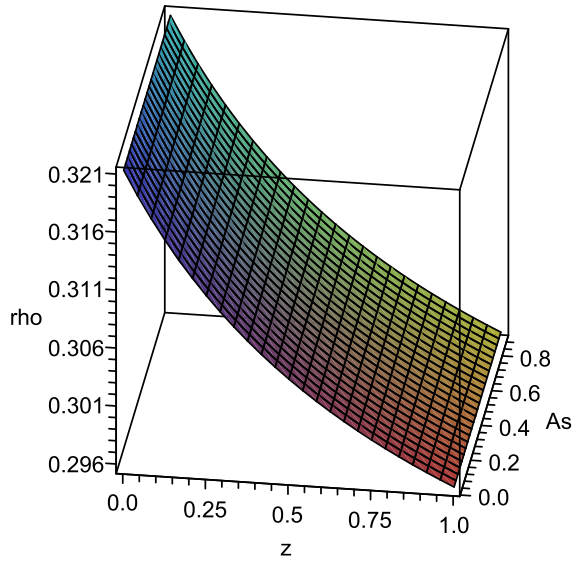


Figure 4: Variation of the effective dark energy versus A_s and redshift. Parameters values are taken from Table 2.

$$\dot{\rho}_{eff} = \frac{-3H_0^2}{\kappa_4^2} \left\{ \frac{3H(1+z)^3(1-A_s)\Omega_{ch}(1+z)^{3\alpha}}{[A_s + (1-A_s)(1+z)^{3\alpha}]^{\frac{\alpha}{\alpha+1}}} + 2\sqrt{\Omega_{r_c}}E(z)[1 + \Omega_\beta E^2(z)]\dot{H}H_0 + 2\sqrt{\Omega_{r_c}}\dot{H}H_0\Omega_\beta E^2(z) \right\} \quad (16)$$

Using equations (13) and (16), we find

$$1 + \omega_{eff} = \frac{\frac{3H(1+z)^3(1-A_s)\Omega_{ch}(1+z)^{3\alpha}}{[A_s + (1-A_s)(1+z)^{3\alpha}]^{\frac{\alpha}{\alpha+1}}} + 2\sqrt{\Omega_{r_c}}E(z)[1 + \Omega_\beta E^2(z)]\dot{H}H_0 + 2\sqrt{\Omega_{r_c}}\dot{H}H_0\Omega_\beta E^2(z)}{3E(z)\left[-2\sqrt{\Omega_{r_c}}E(z)[1 + \Omega_\alpha E^2(z)] + \Omega_{ch}[A_s + (1-A_s)(1+z)^{3(\alpha+1)}]^{\frac{1}{1+\alpha}} + \Omega_\Lambda\right]} \quad (17)$$

Figure 5 shows the plot of $1 + \omega_{eff}$ versus the redshift. The universe enters to the phantom phase smoothly at $z \approx 0.12$. It is important to note that this setup realizes a smooth transition to the phantom phase, the so called *phantom-divide line crossing*. We note that this smooth crossing behavior cannot be realized in the absence of the Chaplygin fluid component. Indeed, without this term, the effective equation of state parameter blows up in the past and as mentioned previously, the effective phantom description breaks down.

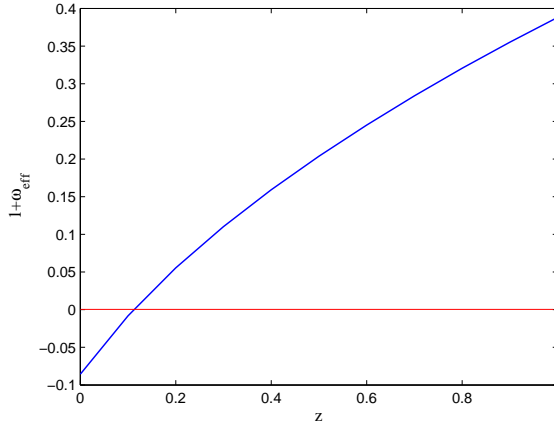


Figure 5: $1 + w_{eff}$ versus the redshift. This model realizes (as a result of the existence of the Chpalygin component on the brane), a smooth crossing of the phantom divide line. Parameters values are taken from Table 2.

Now we study the phantom-like behavior in another perspective: *dynamical screening of the brane cosmological constant* (A. Lue & G. D. Starkman 2004). The normal branch of this model can be described by the following Friedmann equation

$$H^2 = \frac{8\pi G}{3}(\rho_m + \rho_{ch}) + \frac{\Lambda}{3} - \frac{H}{r_c}\left(1 + \frac{8}{3}\beta H^2\right) \quad (18)$$

where Λ is the brane cosmological constant. We rewrite this equation as follows

$$H^2 = \frac{8\pi G}{3}(\rho_m + \rho_{ch}) + \frac{8\pi G}{3}\Lambda^{(eff)}, \quad (19)$$

where by definition

$$\Lambda^{(eff)} = \frac{\Lambda}{3} - \frac{H(1 + \frac{8}{3}\beta H^2)}{r_c}. \quad (20)$$

This equation means that the brane is extrinsically curved so that shortcuts through the bulk allow gravity to screen the effects of the brane cosmological constant at Hubble parameters $H \sim r_c^{-1}$ where r_c is the DGP crossover distance. As a distinctive feature of this model, curvature effect via the Gauss-Bonnet term and presence of the Chaplygin component on the brane contribute in the dynamical screening of the brane cosmological constant. While the role played by the GB term is obvious, the role of the Chaplygin matter is hidden in the definition of the Hubble parameter. This feature leads to a considerable difference relative to the pure DGP case studied in (A. Lue & G. D. Starkman 2004). Figure 6 shows the difference between two scenarios in this respect for some values of Ω_β . Alternatively, we can define also

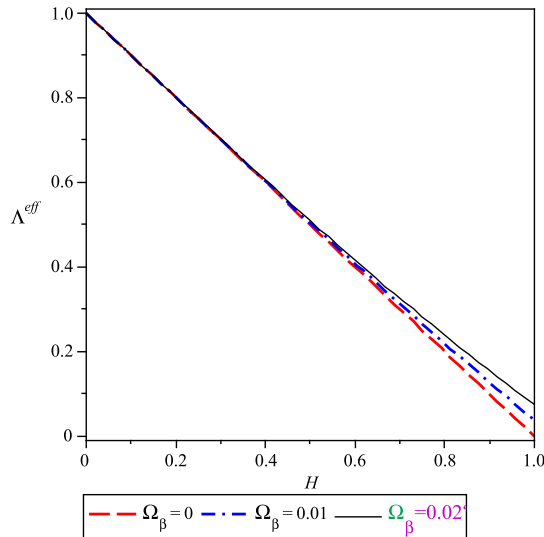


Figure 6: $\Lambda^{(eff)}$ versus the Hubble parameter for different values of Ω_β .

$$\rho_{DE}^{(eff)} = \frac{\Lambda}{3} - \frac{H(1 + \frac{8}{3}\beta H^2)}{r_c}. \quad (21)$$

Figure 7 shows variation of $\rho_{DE}^{(eff)}$ versus z in our proposed setup. It is always positive and grows with cosmic expansion; a typical phantom-like behavior.

4 Observational Constraints

In this section we study the constraints imposed on the GBIG chaplygin model parameters using the observational data such as the gold sample of SNIa combined with the information from the BAO measurement by SDSS and the CMB shift parameter from WMAP7 observations.

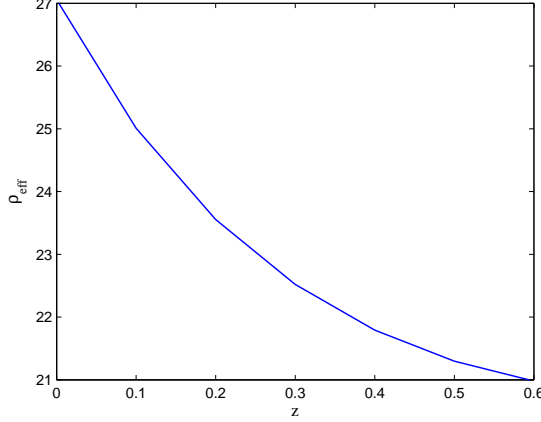


Figure 7: $\rho_{DE}^{(eff)}$ versus the redshift. Parameters values are taken from Table 2.

A: SNIa data

In this section we use the 156 new gold sample supernovae Ia data compiled in (A. G. Riess et al. 2007) to fit the model. This observation directly measures the apparent magnitude m of a supernovae and its redshift z . The apparent magnitude m is related to the luminosity distance d_L of the supernovae through

$$\mu = m - M = \log_{10} d_L + 5 \log_{10} \left(\frac{cH_0}{Mpc} \right) + 25, \quad (22)$$

where M is the absolute magnitude that is believed to be constant for all Type Ia supernovae and d_L is the luminosity distance that in a flat universe can be expressed as follows

$$d_L = (1+z) \int_0^z \frac{dz'}{E(z'; \theta)} \quad (23)$$

where θ denotes the model parameters. From equation (9), the $E(z)$ is given by

$$E(z) = \frac{1}{\Omega_\beta \sqrt{\Omega_{r_c}}} \left[P^{\frac{1}{3}} + \frac{1 - 12\Omega_\beta \Omega_{r_c}}{P^{\frac{1}{3}}} - 1 \right] \quad (24)$$

where

$$P \equiv 18\Omega_\beta \Omega_{r_c} + 54Q\Omega_\beta^2 \Omega_{r_c} - 1 + 6\sqrt{3\Omega_\beta \Omega_{r_c}} \sqrt{16\Omega_\beta \Omega_{r_c}^2 + 18\Omega_\beta \Omega_{r_c} Q + 24\Omega_{r_c} \Omega_\beta^2 Q^2 - \Omega_{r_c} - Q},$$

and

$$Q \equiv \Omega_m (1+z)^3 + \Omega_{ch} [A_s + (1-A_s)(1+z)^{3(\alpha+1)}]^{\frac{1}{1+\alpha}} + \Omega_\Lambda.$$

For the statistical analysis of the supernovae data we perform the χ^2 statistics for the model parameter that is calculated as

$$\chi_{SN}^2(\theta) = \sum_{i=1}^N \frac{[\mu_{obs}(z_i) - \mu_{th}(z_i)]^2}{\sigma_i^2}, \quad (25)$$

Table 1: Priors on the parameter space used in the likelihood analysis.

Parameter	Prior	
Ω_{ch}	0.00 - 1.00	Top Hat
Ω_λ	0.00 - 1.00	Top Hat
Ω_β	0.00 - 1.00	Top Hat
$\Omega_b h^2$	0.02265 ± 0.00059	Top Hat (BBN)

In this relation, $N = 156$ is the number of SNIa data points, μ_{obs} is the observed distance modulus and the σ_i is the uncertainty in the observed distance modulus, which is assumed to be Gaussian and uncorrelated so that the likelihood is proportional to $e^{-\frac{\chi^2}{2}}$. The parameter

$$\bar{M} = 5 \log_{10} \left(\frac{cH_0}{Mpc} \right) + 25,$$

is a *nuisance* parameter and should be marginalized (integrated out). This can be done by following the techniques described in (M. S. Movahed, M. Farhang & S. Rahvar 2009) and can be performed by expanding the χ_{SN}^2 of equation (25) with respect to M as

$$\chi_{SN}^2(\theta) = \tilde{A} - 2M\tilde{B} + M^2\tilde{C} \quad (26)$$

where

$$\tilde{A}(\theta) = \sum_{i=1}^N \frac{[\mu_{obs}(z_i) - \mu_{th}(z_i, M=0, \theta)]^2}{\sigma_i^2}, \quad (27)$$

and

$$\tilde{B}(\theta) = \sum_{i=1}^N \frac{\mu_{obs}(z_i) - \mu_{th}(z_i, M=0, \theta)}{\sigma_i^2}, \quad \tilde{C} = \sum_{i=1}^N \frac{1}{\sigma_i^2}. \quad (28)$$

Equation (25) has a minimum for $M = \frac{\tilde{B}}{\tilde{C}}$ at $\tilde{\chi}_{SN}^2(\theta) = \tilde{A}(\theta) - \frac{\tilde{B}^2(\theta)}{\tilde{C}}$. Using this equation the best fit values of model parameters as the values that minimize $\chi_{SNIa}^2(\theta)$ can be obtained.

For the likelihood analysis we marginalize the likelihood function $L = \exp(-\chi^2/2)$ over h and $\Omega_m = \Omega_b$ where Ω_b is the energy density of the barionic matter. We adopted Gaussian priors such that $h = 0.705$ from the WMAP7 (K. Komatsu et al. 2009) and $\Omega_b = 0.0456$. Table 1 summarizes these priors.

B: CMB shift parameter

We use the CMB data from WMAP7 observation that includes the shift parameter \mathcal{R} and the redshift of the decoupling epoch z_* . The shift parameter \mathcal{R} is related to the angular diameter distance to the last scattering surface, the comoving size of the sound horizon at z_* and the angular scale of the first acoustic peak in the CMB power spectrum of the temperature fluctuations. The CMB shift parameter is approximated by (see for more details R. Lazkoz & E. Majerotto (2007)).)

$$\mathcal{R} = \sqrt{\Omega_m} H_0 r(z_*), \quad (29)$$

where $r(z)$ is the comoving distance to the redshift z defined by

$$r(z) = \int_0^z \frac{1}{H(z)} dz. \quad (30)$$

The constraints on a typical model using CMB shift is obtained from minimization of the quantity

$$\chi_{CMB}^2 = \frac{[\mathcal{R}_{obs} - \mathcal{R}_{th}]^2}{\sigma_{CMB}^2}, \quad (31)$$

where \mathcal{R}_{obs} is the observed value of the CMB shift parameter performed from WMAP7 observation (K. Komatsu et al 2009) and \mathcal{R}_{th} is corresponding to the theoretical value calculated from equation (29).

C: BAO observation

The baryonic acoustic oscillation (BAO) peak detected in the SDSS luminous red Galaxies (LRG) is another tool to test the model against observational data. BAO are described in terms of a dimensionless parameter

$$\mathcal{A} = \sqrt{\Omega_m} \left[\frac{H_0 d_L^2(z; \theta)}{H(z_{sdss}; \theta) z_{sdss}^2 (1 + z_{sdss})^2} \right]^{1/3}. \quad (32)$$

The best fit values of the model parameters can be determined by constructing minimization of the quantity

$$\chi_{SDSS}^2 = \frac{[\mathcal{A}_{obs} - \mathcal{A}_{th}]^2}{\sigma_{sdss}^2}. \quad (33)$$

The observed value \mathcal{A}_{obs} from the LRG is $\mathcal{A}_{obs} = 0.469 \left(\frac{n_s}{0.98} \right)^{-0.35} \pm 0.017$ measured at $z_{sdss} = 0.35$ (R. Lazkoz & E. Majerotto, 2007). Here $n_s = 0.963$ is the spectral index as measured by WMAP seven year observations (K. Komatsu et al 2009). It is important to note that the above observational data are uncorrelated from each other, since they are given by different experiments and methods. Then we can construct a joint analysis of them as

$$\chi_{tot}^2 = \chi_{SN}^2 + \chi_{CMB}^2 + \chi_{SDSS}^2. \quad (34)$$

With these preliminaries, we have obtained the best fit parameters of the GBIG chaplygin model for SNIa data, the joint analysis of the SNIa and CMB, and finally the combined analysis of the total datasets. Table 2 indicates the results of the observational constraints on the free parameters of the model. In figure 8, using the best fit values of the model parameters and observational data from gold sample, we have compared the theoretical predictions of the distance modulus in our model. Figure 9 shows the marginalized relative likelihood with respect to parameter A_S fitted with SNIa gold sample, SNIa+CMB and SNIa+CMB+SDSS experiments. We plot the joint confidence interval of Ω_{r_c} and A_S in figure 10 in 1σ , 2σ and 3σ level of confidence for the mentioned datasets.

Finally and for completeness of discussions, we compare our Chaplygin GBIG scenario with Λ DGP and Λ CDM (see for instance (W. J. Percival et al. 2007) for a general framework). Using the data set in the previous subsections, we obtain the best fit parameters of the Λ DGP

Table 2: The best values for the parameters of GBIG chaplygin model by fitting with SNIa Gold sample, SNIa+CMB and SNIa+CMB+SDSS experiments in a flat background.

Observation	Ω_{r_c}	Ω_β	A_S	Ω_Λ	Ω_{ch}	α	$\chi^2_{min}/N_{d.o.f}$
SNIa(Gold Sample)	0.43	0.11	$0.50^{+0.17}_{-0.48}$	1.45	0.99	0.99	0.923
SNIa(Gold Sample)+CMB	0.53	0.31	$0.12^{+0.15}_{-0.09}$	1.70	0.99	-0.98	0.943
SNIa(Gold Sample)+CMB+SDSS	0.51	0.41	$0.099^{+0.16}_{-0.08}$	1.79	0.99	-0.98	0.992

and Λ CDM models in table 3. Comparing tables 2 and 3, we see that in our model the best fit values (which are given by $\chi^2/N_{d.o.f}$) are more reasonable than Λ DGP and Λ CDM ones on observational ground. In figure 11 we have plotted the marginalized relative likelihood with respect to parameter Ω_m fitted with SNIa gold sample, SNIa+CMB and SNIa+CMB+SDSS experiments. In summary, as tables 2 and 3 show, our Chaplygin GBIG scenario has better agreement with observations than Λ DGP and Λ CDM. In other words, existence of a Chaplygin component on the DGP brane brings the scenario to be more viable in observational viewpoint than the pure Λ DGP or Λ CDM. This is a result of wider parameter space available here which leads to further degrees of freedom.

Table 3: The best values for the parameters of Λ CDM and Λ DGP models by fitting with SNIa Gold sample, SNIa+CMB and SNIa+CMB+SDSS experiments in a flat background.

Observation	Λ CDM model	Λ DGP model
SNIa	$\Omega_m = 0.35^{+0.04}_{-0.04}, \chi^2_{min}/N_{d.o.f} = 0.921$	$\Omega_m = 0.007^{+0.08}, \Omega_{r_c} = 0.22, \chi^2_{min}/N_{d.o.f} = 0.914$
SNIa+CMB	$\Omega_m = 0.34^{+0.03}_{-0.04}, \chi^2_{min}/N_{d.o.f} = 0.926$	$\Omega_m = 0.33^{+0.05}_{-0.12}, \Omega_{r_c} = 0.00, \chi^2_{min}/N_{d.o.f} = 0.926$
SNIa+CMB+SDSS	$\Omega_m = 0.32^{+0.04}_{-0.03}, \chi^2_{min}/N_{d.o.f} = 0.960$	$\Omega_m = 0.34^{+0.02}_{-0.11}, \Omega_{r_c} = 0.00, \chi^2_{min}/N_{d.o.f} = 0.966$

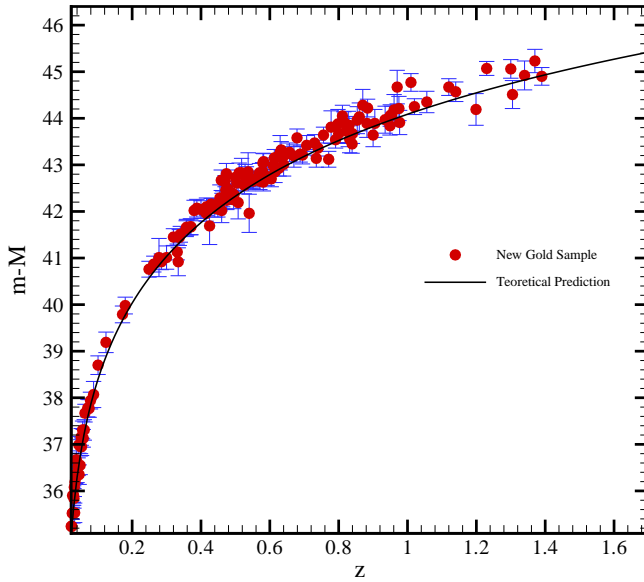


Figure 8: Distance modulus of the SNIa Gold sample versus the redshift. Solid line shows the best fit values with the corresponding parameters of $h = 0.70$, $\Omega_{r_c} = 0.43$ and $A_S = 0.50$ in 1σ level of confidence with $\chi^2_{min} = 141.368$ for GBIG chaplygin model.

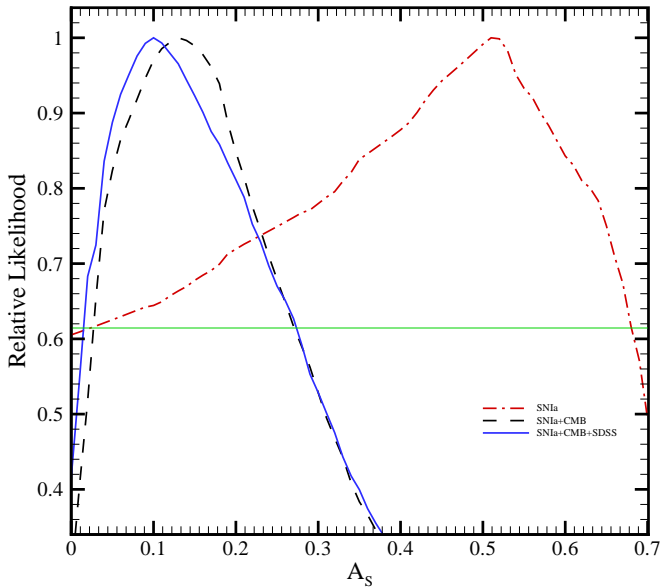


Figure 9: Marginalized relative likelihood with respect to parameter A_S fitted with SNIa gold sample, SNIa+CMB and SNIa+CMB+SDSS experiments. The intersection of the curve with the horizontal solid line is corresponding to the bound with 1σ level of confidence.

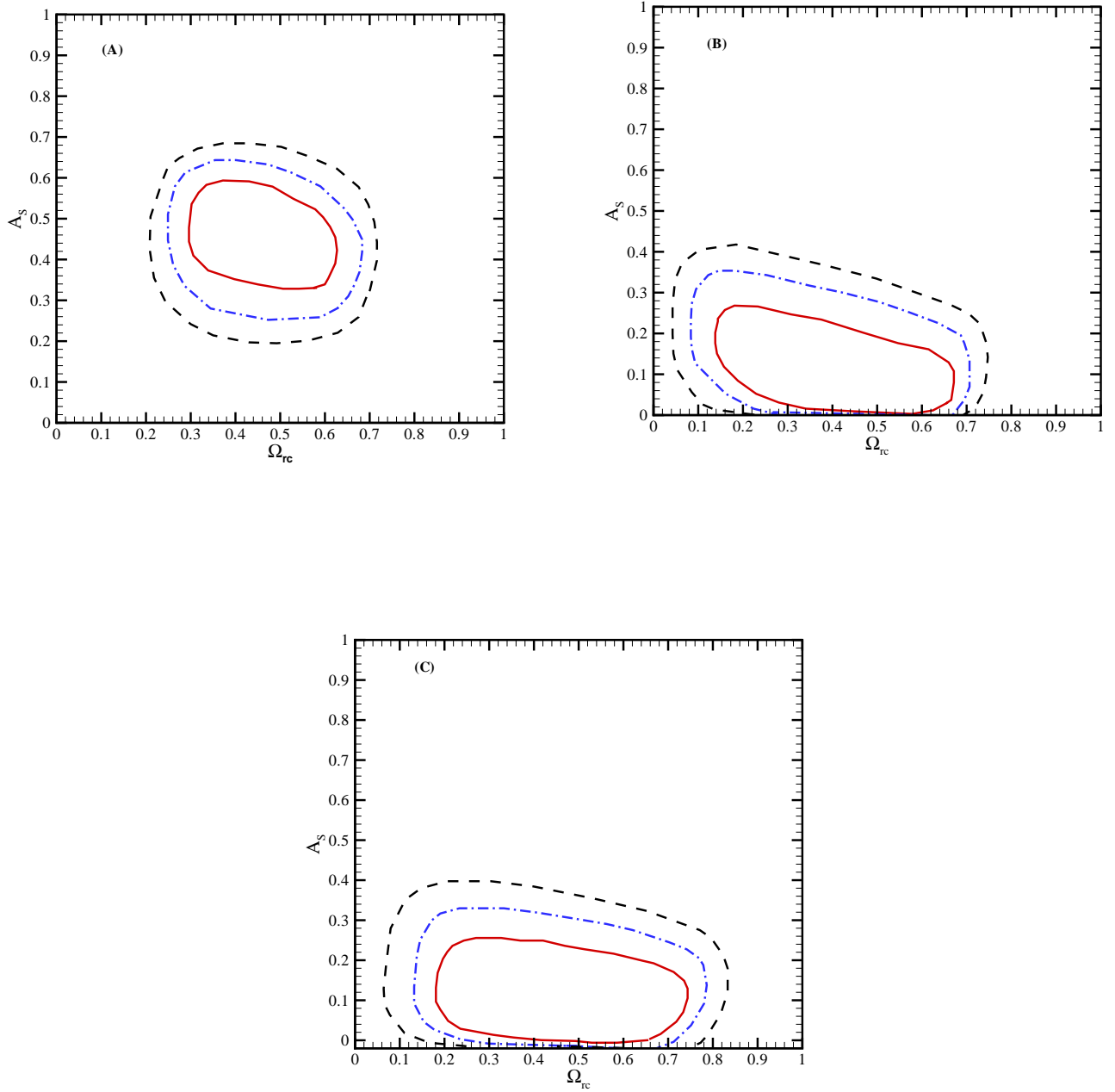


Figure 10: Confidence interval of Ω_{rc} and A_s in 1 σ , 2 σ and 3 σ level of confidence for the SNIa gold data (A), SNIa+CMB joint data (B) and SNIa+CMB+SDSS joint data (C).

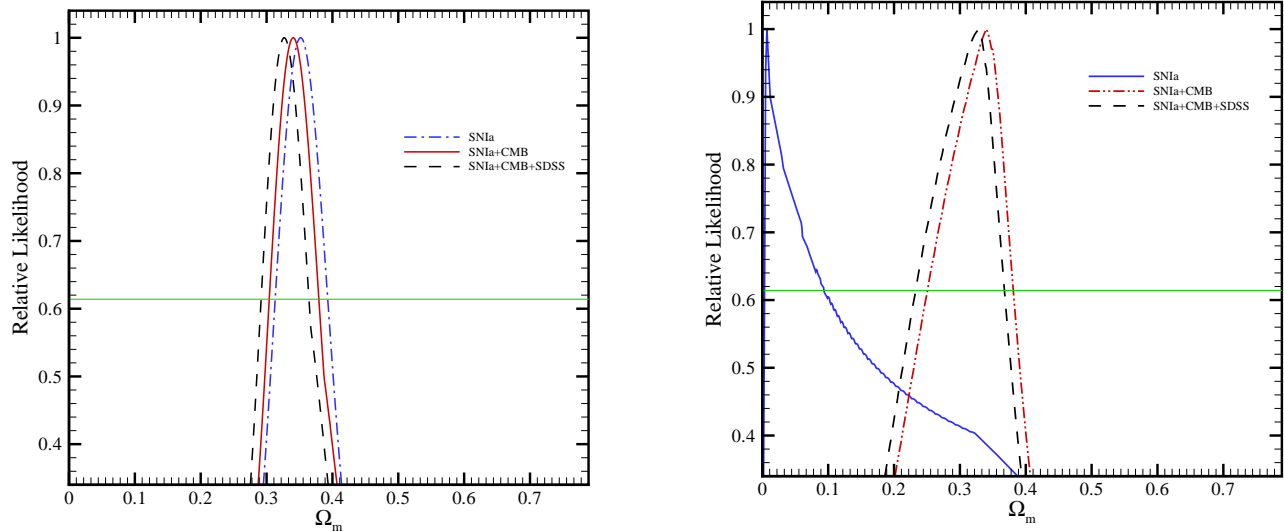


Figure 11: Marginalized relative likelihood with respect to parameter Ω_m fitted with SNIa gold sample, SNIa+CMB and SNIa+CMB+SDSS experiments for Λ CDM (left) and Λ DGP (right) respectively. The intersection of the curve with the horizontal solid line is corresponding to the bound with 1σ level of confidence.

5 Summary and Conclusion

In this paper, we have considered a braneworld induced gravity scenario which contains curvature effect of the Gauss-Bonnet term in the bulk and a Chaplygin gas component in the brane action. We have investigated the cosmological dynamics and the late-time behavior on the brane. We have shown the possibility of getting accelerated expansion in this scenario. We have studied the effective phantom-like behavior on the brane. This behavior can be realized in this scenario and the universe enters into the phantom phase at $z \approx 0.12$. We note that this effective behavior could be deduced also in some braneworld models (such as Λ DGP and pure GBIG scenario) with number of parameters less than our proposed model. However, in such models the effective phantom picture breaks down, and the effective equation of state parameter blows up at a redshift in the past. In our model, inclusion of the Chaplygin gas fluid on the brane saves the phantom-like prescription for a wide range of redshifts. In fact, there is no break down of the effective phantom picture in the presence of the Chaplygin component on the brane. From another perspective, existence of the chaplygin gas component on the brane, leads to a smooth crossing of the phantom divide line by the effective equation of state parameter of the model. We have studied also the notion of dynamical screening of the brane cosmological constant in this generalized setup. Finally, We have confronted the model with observational data from type Ia Supernovae, Cosmic Microwave Background and Baryon Acoustic Oscillations to constraint the model parameter space. The results of comparison of the model parameters space with the observational data are summarized in tables 1 and 2, and corresponding figures 8-10. We have shown that up to the analysis on the parameters space performed here (table 2 and 3), this model has better agreement with observations than the

Λ DGP and Λ CDM. In other words, existence of a Chaplygin component on the DGP brane with curvature effect, brings the scenario to be more viable in observational viewpoint than the pure Λ DGP case. This result is due to the wider parameter space and also further degrees of freedom accessible in the model discussed here.

Acknowledgement

We would like to thank Dr M. Sadegh Movahed for his invaluable contribution in this work. The work of KN is supported partially by the Research Institute of Astronomy and Astrophysics of Maragha, IRAN.

References

- Amendola L., Finelli F., Burigana C., Carturan D., 2003, JCAP, 0307, 005
Bento M. C., Bertolami O., Sen A. A., 2002, Phys. Rev. D, 66, 043507
Bertolami O., Sen A. A., Sen S., Silva P. T., 2004, MNRAS, 353,329
Biesiada M., Godlowski W., Szydlowski M., 2005, ApJ, 622, 28
Bilic N., Tupper G. B., Viollier R. D., 2002, Phys. Lett. B, 535, 17
Bouhmadi-Lopez M., Lazkoz R., 2007, Phys. Lett. B, 654, 51
Bouhmadi-Lopez M., Moniz P. V., 2008, Phys. Rev. D, 78, 084019
Bouhmadi-Lopez M., Moniz P. V., 2009, AIP Conf. Proc, 1122, 201
Bouhmadi-Lopez M., Gonzalez-Diaz P. F., Martin-Moruno P., 2008, Int. J. Mod. Phys. D, 17, 2269
Bouhmadi-Lopez M. et al., 2009, Phys. Rev. D, 79 124035
Bouhmadi-Lopez M. et al., 2010, preprint (arXiv:1002.4783)
Brown R. A., 2007, preprint (gr-qc/0701083)
Brown R. A. et al., 2005, JCAP, 051, 008
Cai R. -G., Zhang H. -S., Wang A., 2005, Commun. Theor. Phys, 44, 948
Caldwell R. R., 2002, Phys. Lett. B 545, 23
Caldwell R. R., Kamionkowski M., Weinberg N. N., 2003, Phys. Rev. Lett, 91, 071301
Chimento L. P., Lazkoz R., Maartens R., Quiros I., 2006, JCAP, 0609, 004
Davis, T. M. et al. 2007, Astrophys. J., 666, 716
Deffayet C., 2001, Phys. Lett. B, 502, 199
Deffayet C., Dvali G., Gabadadze G., 2002, Phys. Rev. D, 65, 044023
Dev A., Alcaniz J. S., Jain D., 2003, Phys. Rev. D, 67, 023515
Dvali G., Gabadadze G., Porrati M., 2000, Phys. Lett. B, 485, 208
Dvali G., Gabadadze G., Kolanovic M., Nitti F., 2002, Phys. Rev. D 65, 208, 024031
He J. -H., Wang B., Papantonopoulos E., 2007, Phys. Lett. B, 654, 133
Heydari-Fard M., Sepangi H. R., 2008, Phys. Rev. D, 78, 064007
Kamenshchik A. Y., Moschella U., Pasquier V., 2001, Phys. Lett. B, 511, 265
Komatsu K. et al., 2009, AIP Conf. Proc., 1129, 53
Kofinas G., Maartens R., Papantonopoulos E., 2003, JHEP, 0310, 066
Komatsu E. et al., [arXiv:1001.4538]
Lazkoz R., Majerotto E., 2007, JCAP, 0707, 015
Lue A., 2006, Phys. Rept, 423, 48
Lue A., Starkman G. D., 2004, Phys. Rev. D, 70, 101501
Maartens R., Majerotto E., 2006, Phys. Rev. D, 74, 023004
Maeda H., Sahni V., Shtanov Y., 2007, Phys. Rev. D, 76, 104028

Mohseni Sadjadi H., 2009, preprint (arXiv:0909.1002)
Movahed M. S., Farhang M., Rahvar S., 2009, Int. J. Theor. Phys, 48, 1203
Nozari K., Aliopur N., 2009, Europhys. Lett, 87, 69001
Nozari K., Azizi T., Setare M. R., 2009, JCAP, 10, 022
Nozari K., Fazlpour B., 2008, JCAP, 0806, 032
Nozari K., Rashidi N., 2009a, JCAP, 0909, 014
Nozari K., Rashidi N., 2009b, Int. J. Theor. Phys, 48, 2800
Percival W. J. et al., 2007, MNRAS, 381, 1053
Riess A. G. et al., 2007, APJ, 659, 98
Roos M., 2007, preprint (arXiv:0704.0882)
Roos M., 2008a, preprint (arXiv:0704.0882)
Roos M., 2008b, Phys. Lett. B, 666, 420
Sahni V., 2005, (arXiv:astro-ph/0502032)
Sahni V., Shtanov Y., 2003, JCAP, 0311, 014
Yurov A. V. et al., 2008, Grav. Cosmol, 14, 205
Zhang H., Zhu Z. -H., 2006, Phys. Rev. D, 73, 043518
Zhang H., Zhu Z. -H., Yang L., 2009, Mod. Phys. Lett. A, 24
Zhang X., Wu F., Zhang J., 2006, JCAP, 0601, 003